

超冷原子冷却用集成全光纤 1064 nm 激光系统的研制

谢昱^{1,2}, 梁昂昂^{1,2}, 李文文^{1,2}, 黄名山^{1,2}, 汪斌^{1**}, 刘亮^{1*}

¹中国科学院上海光学精密机械研究所航天激光工程部, 上海 201800;

²中国科学院大学材料科学与光电技术学院, 北京 100049

摘要 深度冷却是超冷原子制备过程的关键步骤,是探寻极低温度的关键技术。详细阐述了一种用于⁸⁷Rb原子深度冷却的集成化全光纤 1064 nm 激光系统的研制方案。激光器采用两级主振荡功率放大的方案,将单一种子源信号进行放大、分束和调控,输出 4 路具备独立控制的激光,作为制备超冷量子气体的交叉光阱的光源。经测试,激光器在功率、稳定性、噪声等各方面满足原子深度冷却的实验需求。在地面条件下进行的两级深度冷却预实验中,获得了 10 nK 以下的初步实验结果,这验证了激光器具备实现超冷原子深度冷却所需的全部功能。激光器集成了种子源、放大器和全功能光学平台的功能,其内部模块采用全光纤器件研制,具有集成化、数字化、高稳定、免调试、易维护等优点,经过简易改造能够应用于远程遥控和遥测的超冷原子项目中。

关键词 激光光学; 激光囚禁; 玻色-爱因斯坦凝聚体; 光纤激光器; 激光冷却

中图分类号 O515 文献标志码 A

DOI: 10.3788/AOS221183

1 引言

超低温一直是物理研究与技术发展的关键目标与驱动力。1985 年激光冷却技术的发明将稀薄原子气体的温度极限推进到了 μK 量级^[1-5],为人类带来了冷原子干涉仪^[6-8]等精密测量仪器。1995 年的蒸发冷却实验成功实现了 nK 量级的冷却温度,更是开拓了对玻色-爱因斯坦凝聚体(BEC)^[9-12]和简并费米气体(DFG)^[13-14]的实验研究,进一步实现了用于研究复杂量子多体问题的光晶格量子模拟^[15-20]。

为了排除重力的影响、更进一步获得低于 1 nK 的超低温,科学家们相继提出了 Quantus 落塔^[21]、抛物线飞机^[22]、MAIUS 声速火箭^[23-24]和冷原子实验室(CAL)国际空间站载荷^[25]等微重力实验方案,并利用小型化原子芯片等装置实现了动能等效温度小于 1 nK 的超冷原子气体。2021 年,Rasel 小组^[26]利用 BEC 四极振荡模将一维动量转移至其他两个维度上,并利用脉冲冲击冷却(DKC)的方法冷却剩下两个维度,创造了等效温度低于 38 pK 的超低温极限。2022 年,Gaaloul 等^[27]同样利用 DKC 的方法在轨获得了 50 pK 的超低温样本。

为了与微重力设备兼容,上述实验方案大部分采用小型化的原子芯片,利用磁透镜 DKC 进行深度冷却。2013 年陈徐宗小组^[28]提出了一个应用于微重力

条件下基于全光方法进行深度冷却的实验方案。该方案采用两对 1064 nm 远失谐光阱(FORT),相继进行蒸发冷却和绝热膨胀冷却,通过直接蒙特卡罗模拟算法计算得出在微重力环境中可以获得低于 100 pK 的超冷原子气体的结论。相比于 DKC,这种两级冷却(TSC)方法能够避免阱频率各向异性导致的冷却效率的降低,从而实现更低的冷却温度,因此更具有应用潜力^[29-30]。通过磁托举方法,2018 年 Luan 等^[30]对⁸⁷Rb 原子进行了地面模拟微重力实验,获得了温度低达 3 nK 的⁸⁷Rb BEC。

空间超冷原子物理实验采用上述 TSC 实验方案作为超低温冷原子制备的关键技术路线,并基于此进行了如下改进:增大光阱光功率动态范围和关断比,进一步降低冷却温度;采用 4 路独立控制的光阱激光,避免单路激光复用导致的光功率不平衡等问题;系统具备集成化、小型化、高可靠性特性,满足实验设备工程化需求。

为了实现在轨全光深度冷却,在前期工作^[31-34]的基础上,开发了一套集成化全光纤 1064 nm 光阱激光系统。激光器内部集成了种子源、光功率开关以及放大、调控、闭环反馈等功能,激光器与物理系统通过光纤进行连接,提供满足 TSC 冷却实验需要的 4 路交叉光阱激光。相比于常规地面实验室常见的 FORT 光路设

收稿日期: 2022-05-23; 修回日期: 2022-06-16; 录用日期: 2022-06-29; 网络首发日期: 2022-07-09

基金项目: 国家自然科学基金(U1730126)、中国科学院青年创新促进会

通信作者: *liang.liu@siom.ac.cn; **wangbin@siom.ac.cn

计^[35-36],全光纤链路具有高稳定、免调试、易维护等优点,充分满足空间站等远程遥控项目的应用需求。本文描述了激光器的光学设计,通过指标分解及实验验证,提供了一套标准的设计实施流程,以为后续工作提供借鉴和参考。

2 理论分析

TSC 方案采用不同功率的两对 1064 nm 连续光构成阱深和阱体积各不相同的 FORT,按照光腰大小可将光阱分为细腰光阱和粗腰光阱。对于细腰 w 相同、传播方向垂直的一对高斯光束构成的光阱,其势阱空间分布为

$$U(x, y, z) = -U_z \exp\left[-\frac{2(x^2 + y^2)}{w^2}\right] - U_x \exp\left[-\frac{2(y^2 + z^2)}{w^2}\right], \quad (1)$$

式中: U_z 和 U_x 分别是沿 z 和 x 方向传播的光阱深度; $U_{z(x)} = \frac{3\pi c^2 P_{z(x)}}{2\omega_0^3 w^2} \left(\frac{\Gamma_{\text{nature}}}{\omega_0 - \omega_{\text{laser}}}\right)$, $P_{z(x)}$ 为沿 $z(x)$ 方向传播的光阱的光功率, c 为真空光速, Γ_{nature} 为原子上能级自然线宽, ω_0 为共振跃迁频率, ω_{laser} 为光阱工作频率。

根据目前的实验参数,细腰光阱阱深需要在 500 μK ~100 nK 范围内连续可调,而粗腰光阱阱深要求覆盖 1 nK~100 nK 范围,对应的两类光阱的功率不小于 5 W 和 100 mW,要求关断比不小于 60 dB 和 40 dB。

两级冷却期间,光阱的功率波动会导致加热,基于参量激发理论对激光器相对功率稳定度 ϵ_0 进行估计^[37]:

$$\epsilon_0 = \sqrt{\int_0^\infty d\nu_{\text{trap}} S_\epsilon(2\nu_{\text{trap}})} = \sqrt{\int_{\nu_{\text{lower}}}^{\nu_{\text{upper}}} d\nu_{\text{trap}} \frac{1}{T_1 \pi^2 \nu_{\text{trap}}^2}}, \quad (2)$$

式中: $S_\epsilon(2\nu_{\text{trap}})$ 为阱频率 ν_{trap} 的 2 倍处的噪声功率谱密度; T_1 是预期的原子寿命(加热率的倒数); ν_{lower} 和 ν_{upper} 分别为二倍阱频率的上下限,由相应的实验光阱阱频率范围决定。假设原子寿命 $T_1 \geq 100$ s,相应的满功率下细腰、粗腰光阱光功率稳定度静态指标分别为 $\epsilon_{0, \text{thin}} \leq 2.5 \times 10^{-3}$ 和 $\epsilon_{0, \text{wide}} \leq 2.13 \times 10^{-2}$ 。当光阱光功率反馈带宽大于冷却阶段的功率扫描采样频率时,可以将每个采样点视为一段静态过程,由此可以将满功率下光阱光的静态光功率稳定性指标视为两级冷却期间的动态指标。

此外,航天工程对集成化、小型化、数字化具有较高要求,商用激光器难以满足。结合上述实验要求,研制了一套用于超冷原子深度冷却的集成化全光纤 1064 nm 激光器。

3 激光系统光学设计

3.1 激光系统模块设计

总体上,激光器采用分束放大的方案,即采用“前级放大器+分束+功率控制+后级放大器”对单一种子源进行多路高功率放大与大动态范围控制,使其满足原子冷却实验的需求。种子源选用具有连续输出能力的单模窄线宽 1064 nm 激光管。光功率放大器采用光纤主振荡功率放大(MOPA)方案。光功率控制采用光纤耦合声光调制器(AOM)。

激光系统由全保偏光纤器件组成,光纤链路如图 1 所示,依照功能可分为高质量种子源(图 1 左侧部分)和高功率放大(图 1 右侧部分)等两大模块。单一光源

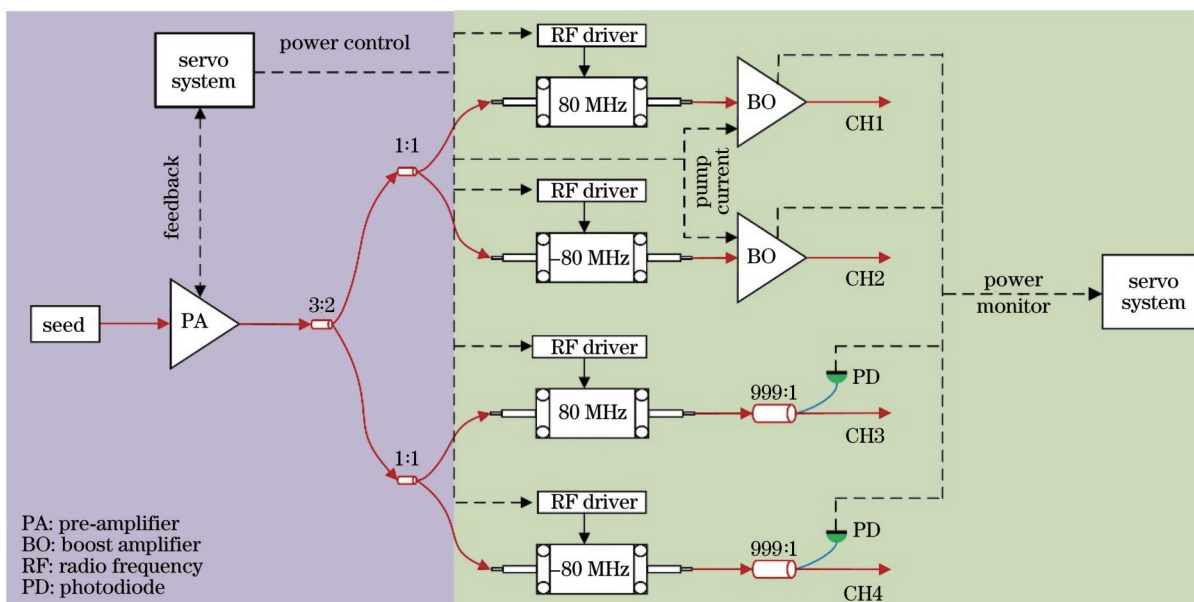


图 1 1064 nm 激光器光学原理设计图

Fig. 1 Optical principle design of 1064 nm laser

小信号种子光经 MOPA 器件、光纤分束器、光纤 AOM 等产生 CH1~CH4 这 4 路功率可调谐的 1064 nm 远失谐光阱激光。其中 CH1、CH2 作为高功率细腰光阱光, CH3、CH4 作为低功率粗腰光阱光。

高质量种子源模块用于产生后续光学系统所需的稳定可靠的光源, 包含种子源、高增益预放大器 (PA) 和光纤分束器三个部分。其中, 种子源 (PL-DFB-1064-A1, LD-PD 公司) 输出中心波长为 1064 nm、功率为 50 mW 的种子光。PA 对小信号种子光进行高增益光功率放大, 实现大于 2 W 的高稳定闭环反馈输出。PA 输出信号经过两级分束, 产生功率比满足 3:3:2:2 的 4 路支路信号, 其中前两路作为细腰光阱光源, 后两路作为粗腰光阱光源。

高功率放大模块起到放大、功率控制和监测的作用, 使得输出信号在功率、动态范围和稳定性等方面均能满足实验需求。高功率放大模块包含功率控制级和功率监测级两个组成部分。根据输出需求的不同, 每一路的功率控制级设计方案也略有差异。4 路光阱光均采用光纤 AOM 进行功率控制, 同时对成对信号引入了 160 MHz 的频率差, 以避免光阱交叠处产生的干涉条纹对原子的加热 (光阱的阱频率一般在 kHz 量级, 远低于 160 MHz)。特别地, 在 CH1、CH2 支路 AOM 后再插入一级高功率主放大器 (BO), 以实现细腰光阱光大于 5 W 的输出需求。为了满足输出功率的稳定性要求, 在各路激光输出前, 利用高分束比的分光器对输出功率进行采样, 采用 PD 进行功率监测, 并将功率采

样信号通过伺服系统反馈至 AOM 射频源或 BO 泵浦电流驱动上, 实现输出光功率的闭环反馈控制。

3.2 光纤放大器设计

MOPA 器件选用发射波段为 1000~1100 nm 的掺镱光纤 (YDF) 作为增益介质, 同时选用 976 nm 光栅锁波长 LD 对 YDF 进行包层正向泵浦。如此选择的原因是: 1) 增益光纤对 976 nm 光波具有最大的吸收系数, 能减短 YDF, 抑制受激布里渊散射 (SBS) 阈值, 提高输出功率; 2) 泵浦光波长锁定能够有效避免敏感波段波长抖动, 导致泵浦效率的降低, 提高输出稳定性; 3) 正向泵浦具有较小的噪声系数, 能够有效提高输出光束的信噪比。

对于高功率光路 CH1、CH2, 采用两级 MOPA 方案, 通过 PA 与 BO 的配合, 缩短单级增益光纤长度, 提高 SBS 阈值, 抑制其对输出线宽的影响, 通过中间级滤波等处理, 减少自发辐射放大 (ASE) 噪声在链路中传播, 提高输出信号的信噪比和光谱纯度。

PA 与 BO 两类放大器结构如图 2 所示, 均采用了单级 MOPA 方案。信号通过分束器后, 进行功率监测, 将其反馈到泵浦 LD 供电控制上, 避免放大器空载导致损坏。随后, 利用功率耦合器 (PC) 将信号光与泵浦光进行合束, 一同输入 YDF 进行饱和增益放大。放大后, 利用包层泵浦除去器 (CPS) 上涂敷的高折射率包层材料, 除去残余在包层中的高功率泵浦信号, 进而提高输出光谱纯度。最后通过光纤光隔离器 (ISO) 隔离回波, 避免自激振荡对光纤器件的损坏。为了进一

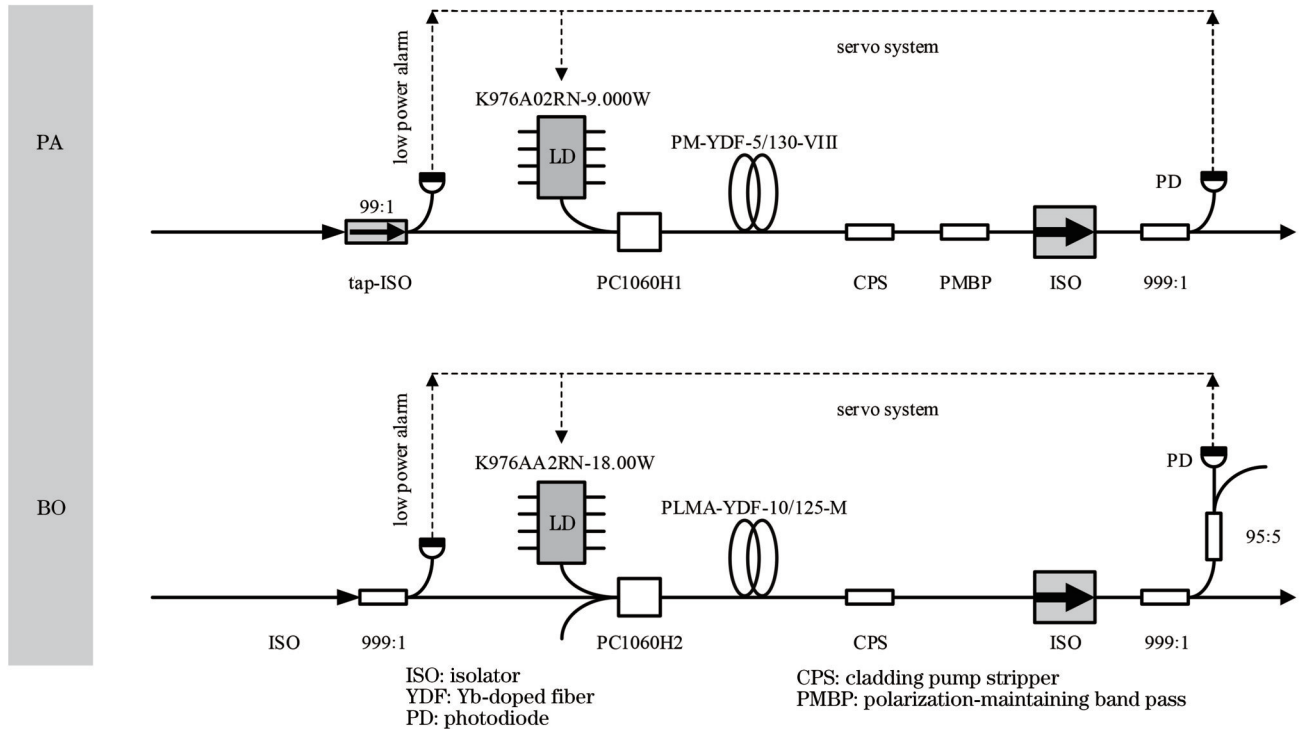


图 2 光功率光纤放大级 MOPA 结构

Fig. 2 MOPA structure of optical power fiber amplification stage

步提高输出稳定性,采用分束器和光电探测器(PD)对输出信号进行采样,通过伺服系统反馈至泵浦LD,对输出功率进行反馈控制。

根据应用场景的不同,两者设计也略有不同。PA输入级采用了具备隔离功能的隔离分束器(tap-ISO)以有效隔离放大器的后向回波,防止损坏种子源。由于前级PA输出具备了隔离功能,所以BO输入级仅使用高分束比的分束器即可防止放大器空载,能够降低ISO带来的插入损耗。另一处不同在于,在CPS后级PA添加了一段滤波带宽为 ± 2 nm的保偏带通滤波片(PMBP)作为中间级滤波,提高PA输出的信噪比,抑制ASE等噪声在光纤链路中的传播。

4 结果与讨论

4.1 部件测试

MOPA器件是实现光功率放大的唯一器件,同时也是细腰光栅高功率控制的重要组成部分,通过对三路放大器进行逐级测量,确定了放大器工作点和驱动电流控制曲线。

测得不同泵浦功率下MOPA器件的开环功率曲线[图3(a)]和各级LD的泵浦功率随电流的变化曲线[图3(b)]。图中方点线、圆点线和三角点线分别是PA、BO-CH1和BO-CH2的测试数据。放大器的泵浦阈值功率较低,增益曲线线性光滑,未出现明显损伤及饱和现象,最大输出功率均能满足激光器设计需求。

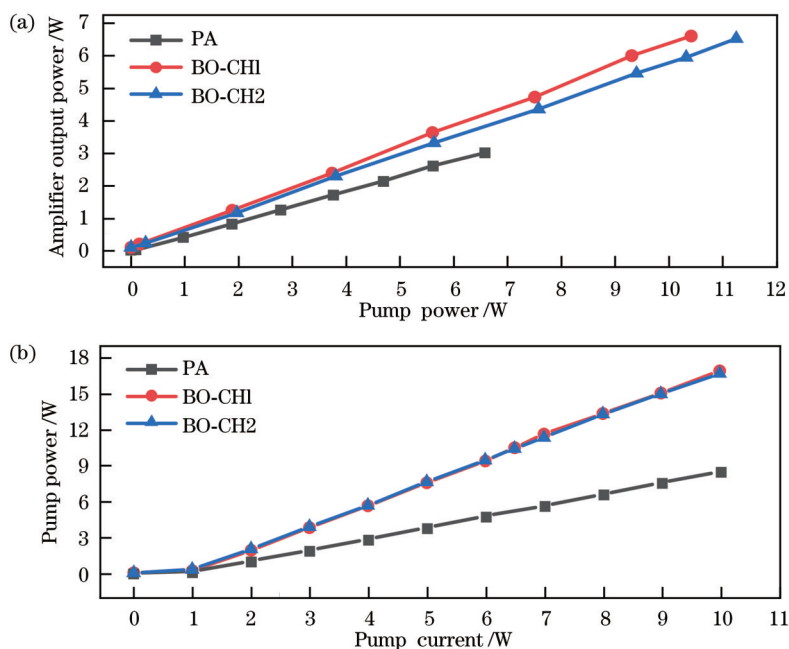


图3 MOPA输出功率随PA和BO的泵浦功率的变化,以及放大器泵浦功率随泵浦电流的变化。(a) MOPA输出功率随PA和BO的泵浦功率的变化;(b)放大器泵浦功率随泵浦电流的变化

Fig. 3 Pump power of PA and BO varying with MOPA output power, and pump power of amplifier varying with pump current.

(a) Pump power of PA and BO varying with MOPA output power; (b) pump power of amplifier varying with pump current

对放大器输出信号进行光谱采集,得到图4所示的谱线数据。比较图中两类放大器的输出光谱特征可

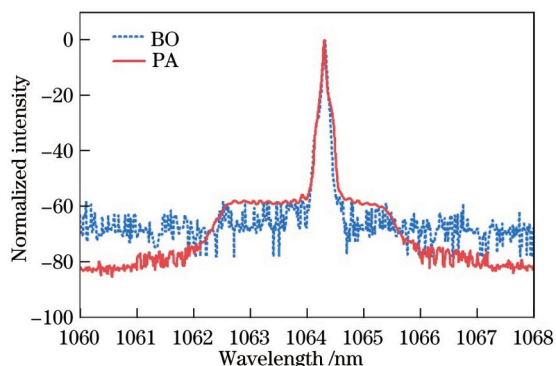


图4 放大器输出信号的光谱曲线

Fig. 4 Spectral curves of output signal of amplifier

以发现,相比于种子源,经过PA(实线)和BO(短点线)放大后的信号没有产生明显的加宽和噪声,边模抑制比均达到了 -56 dB的水平。特别地,中间级滤波器的加入有效抑制了 -10 dB带外噪声,提高了PA预放大光的信噪比,提高了后级放大效率。

测量了不同调制电压下AOM的输出光功率,得到了如图5所示的关系曲线,利用曲线对光栅光输出功率进行标定,以实现深度冷却末期对光栅阱深的精确控制。选用 $0\sim 500$ mV的调制电压的单调增区间(图中高亮区域)作为光栅光功率的有效控制区间。此外,还可以通过匹配不同的控制电压来平衡成对光栅光的输出光功率,防止超冷原子在冷却过程中功率不平衡导致的加热。由图5可知,控制区间内最大关断比分别为 48.55 dB和 52.7 dB,满足粗腰光栅光对光

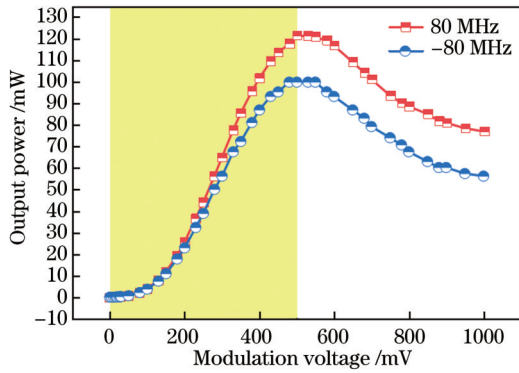


图5 AOM输出光功率随调制电压的变化曲线

Fig. 5 AOM output optical power varying with modulating voltage

功率关断比的实验要求。

4.2 集成测试

组装完成的激光器可分为两个标准机柜抽屉,其中光学&电控系统整机高度为178 mm,供电模块高度为44.5 mm,较常规1.2 m×1.5 m的小型光学实验平台尺寸更便于集成,可以满足各类可搬运需求。完成系统集成后,对激光器输出性能和稳定性进行了测试。

对光阱输出光功率和关断比进行的测量与统计结果如表1所示,RSD为相对标准差, P_{on} 为最高出光功率, P_{off} 为最低出光功率。其中,细腰、粗腰光阱光的标准输出功率分别达到5.4 W和0.16 W,光功率开关比($R_{on/off}$)分别达到了60 dB和45 dB以上,光功率长期漂移低于 6×10^{-3} ,短期稳定性优于 $7.2 \times 10^{-5} @ 1$ s。

表1 激光器输出光功率与闭环稳定性

Table 1 Output power of laser and closed-loop stability

Channel	P_{on} / W	P_{off} / μ W	$R_{on/off}$ / dB	RSD at 1 h / 10^{-3}	RSD at 1 s / 10^{-5}
CH1	5.41	5.2	60.1	6	7.2
CH2	5.40	2.2	63.9	5	8.3
CH3	0.161	4.7	45.4	2	5.5
CH4	0.167	4.6	45.6	3	6.3

经过进一步的测量,得到了满负荷输出时光阱光功率相对强度噪声(RIN)谱线,如图6所示。图中虚线为由式(2)推导出的原子寿命 $T_1 > 100$ s所对应的RIN值曲线,短点线为细腰光阱光的RIN谱线,而实线为粗腰光阱光的RIN谱线。可以发现由于末级采用了带宽为10 kHz的光功率反馈控制,粗细腰光阱光的RIN曲线不存在明显的差异,且全频域均优于需求曲线。

特别地,在如图6插图所示的高亮区域($\nu_{lower} \sim 10$ kHz),激光器RIN值显著低于需求曲线,从而避免了参量激发导致的严重加热和原子数损失现象。利用式(2)定量计算两束光阱光的功率抖动,其中细腰光阱光的功率稳定度静态指标为 $\epsilon_{thin} = 5.1 \times 10^{-4}$ ($\nu_{lower} = 160$ Hz),而粗腰光阱光的功率稳定度静

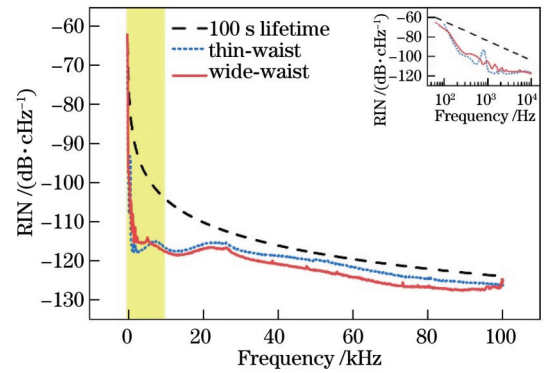


图6 两类光阱满功率输出时的RIN谱线(插图为DC到10 kHz阴影区域的噪声谱)

Fig. 6 RIN spectral lines of two optical dipole traps with full output power (inset is detail of shadow area from DC to 10 kHz)

态指标为 $\epsilon_{wide} = 7.9 \times 10^{-3}$ ($\nu_{lower} = 1$ Hz)。

以上测试结果完全满足TSC深度冷却实验对光功率、关断比和噪声抑制的各项需求。

4.3 实验验证

将上述激光系统集成至超冷原子物理实验柜地面样机的物理系统上,并进行了初步的 ^{87}Rb 的地面模拟TSC深度冷却实验。实验包括了预冷却阶段(MOT & molasses)、光阱装载阶段(FORT loading)、蒸发冷却阶段(1st eva. cooling)和绝热膨胀阶段(2nd adia. cooling)等,流程如图7所示。实验周期内,光阱光功率依照图中短点线和实线的方式进行扫描,采样频率为1 kHz。

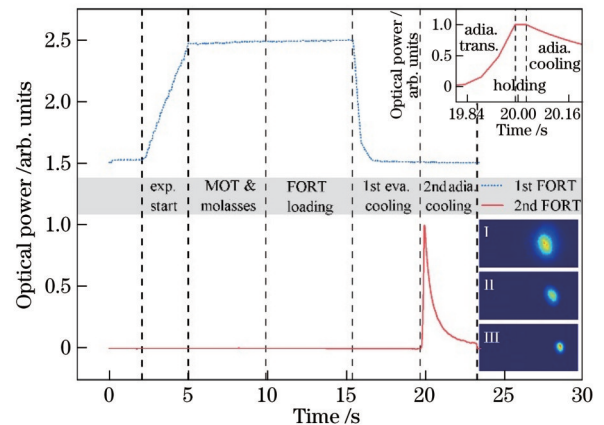


图7 细腰光阱(1st FORT)与粗腰光阱(2nd FORT)的光功率曲线(右上角插图为二级绝热膨胀冷却阶段细节展开图,图I为细腰光阱蒸发冷却结束时的原子光学密度,图II是粗腰光阱保持结束时的原子光学密度,图III是绝热膨胀冷却结束时的原子光学密度)

Fig. 7 Optical power curves of 1st FORT and 2nd FORT (inset is details of 2nd adia. cooling stage, subfigures I, II, and III are atom optical density of end of 1st eva. cooling for 1st FORT, end of holding for 2nd FORT, and end of 2nd adia. cooling)

在粗腰光阱绝热膨胀冷却各阶段采用 20 ms 的飞行时间的吸收成像对深度冷却效果进行分析,得到如图 7 中插图 I、II、III 所示的光学厚度(OD)分布。插图 I 中原子处于蒸发冷却结束阶段,此时 BEC 等效温度降低至 33 nK;插图 II 对应粗腰光阱保持阶段结束,此时系统温度进一步降低至 14 nK;插图 III 是进行绝热膨胀冷却后的结果,温度进一步降低至 10 nK。以上实验结果说明本文所设计的光阱激光器具备进行实验的条件,满足实验要求。

5 结 论

详细阐述了一种用于 ^{87}Rb 原子冷却的集成式全光纤 1064 nm 激光系统的研制和测试。该系统利用全光纤器件实现了种子源、光功率放大、光功率调控和输出反馈等功能,具备小型化、集成化的特点,适合各类具有搬运需求的超冷原子应用中。激光器采用了两级分离式的 MOPA 方案,利用后置的高功率放大器实现了两路 5 W 和两路 160 mW 的大跨度的光功率独立输出。配合严格的时序控制,联合了 BO 与光纤 AOM 的功率控制能力,实现了 60 dB 的大动态范围功率扫描。通过有效的反馈控制措施,将相对强度噪声降低到 5×10^{-4} 的水平。后续的地面模拟微重力 TSC 实验中得到了低于一般全光蒸发冷却能够达到的 10 nK 量级的超低温,结果证明该激光系统充分满足 TSC 深度冷却实验对 4 束冷却光在功率、控制以及稳定性上的要求,在后续空间超冷原子物理实验柜在轨实验中起到了工程验证的作用。

参 考 文 献

- [1] Prodan J V, Phillips W D, Metcalf H. Laser production of a very slow monoenergetic atomic beam[J]. *Physical Review Letters*, 1982, 49(16): 1149-1153.
- [2] Lett P, Watts R, Westbrook C, et al. Observation of atoms laser cooled below the doppler limit[J]. *Physical Review Letters*, 1988, 61(2): 169-172.
- [3] Chu S, Hollberg L, Bjorkholm J E, et al. Three-dimensional viscous confinement and cooling of atoms by resonance radiation pressure[J]. *Physical Review Letters*, 1985, 55(1): 48-51.
- [4] Raab E L, Prentiss M, Cable A, et al. Trapping of neutral sodium atoms with radiation pressure[J]. *Physical Review Letters*, 1987, 59(23): 2631-2634.
- [5] Dalibard J, Cohen-Tannoudji C. Laser cooling below the Doppler limit by polarization gradients: simple theoretical models [J]. *Journal of the Optical Society of America B*, 1989, 6(11): 2023-2045.
- [6] Ménot V, Vermeulen P, Le Moigne N, et al. Gravity measurements below 10^{-9} g with a transportable absolute quantum gravimeter[J]. *Scientific Reports*, 2018, 8: 12300.
- [7] Wynands R, Weyers S. Atomic fountain clocks[J]. *Metrologia*, 2005, 42(3): S64-S79.
- [8] Campbell S L, Hutson R B, Marti G E, et al. A Fermi-degenerate three-dimensional optical lattice clock[J]. *Science*, 2017, 358(6359): 90-94.
- [9] Anderson M H, Ensher J R, Matthews M R, et al. Observation of Bose-Einstein condensation in a dilute atomic vapor[J]. *Science*, 1995, 269(5221): 198-201.
- [10] Davis K B, Mewes M O, Andrews M R, et al. Bose-Einstein condensation in a gas of sodium atoms[J]. *Physical Review Letters*, 1995, 75(22): 3969-3973.
- [11] Cornell E A, Wieman C E. Nobel lecture: Bose-Einstein condensation in a dilute gas, the first 70 years and some recent experiments[J]. *Reviews of Modern Physics*, 2002, 74(3): 875-893.
- [12] Ketterle W. Nobel lecture: when atoms behave as waves: Bose-Einstein condensation and the atom laser[J]. *Reviews of Modern Physics*, 2002, 74(4): 1131-1151.
- [13] DeMarco B, Jin D. Onset of Fermi degeneracy in a trapped atomic gas[J]. *Science*, 1999, 285(5434): 1703-1706.
- [14] DeMarco B, Papp S B, Jin D S. Pauli blocking of collisions in a quantum degenerate atomic Fermi gas[J]. *Physical Review Letters*, 2001, 86(24): 5409-5412.
- [15] Greiner M, Mandel O, Esslinger T, et al. Quantum phase transition from a superfluid to a Mott insulator in a gas of ultracold atoms[J]. *Nature*, 2002, 415(6867): 39-44.
- [16] Lewenstein M, Sanpera A, Ahufinger V, et al. Ultracold atomic gases in optical lattices: mimicking condensed matter physics and beyond[J]. *Advances in Physics*, 2007, 56(2): 243-379.
- [17] Bloch I, Dalibard J, Zwerger W. Many-body physics with ultracold gases[J]. *Reviews of Modern Physics*, 2008, 80(3): 885-964.
- [18] Jördens R, Strohmaier N, Günter K, et al. A Mott insulator of Fermionic atoms in an optical lattice[J]. *Nature*, 2008, 455(7210): 204-207.
- [19] Schneider U, Hackermüller L, Will S, et al. Metallic and insulating phases of repulsively interacting fermions in a 3D optical lattice[J]. *Science*, 2008, 322(5907): 1520-1525.
- [20] Billy J, Josse V, Zuo Z C, et al. Direct observation of Anderson localization of matter waves in a controlled disorder[J]. *Nature*, 2008, 453(7197): 891-894.
- [21] van Zoest T, Gaaloul N, Singh Y, et al. Bose-Einstein condensation in microgravity[J]. *Science*, 2010, 328(5985): 1540-1543.
- [22] Geiger R, Ménot V, Stern G, et al. Detecting inertial effects with airborne matter-wave interferometry[J]. *Nature Communications*, 2011, 2: 474.
- [23] Becker D, Lachmann M D, Seidel S T, et al. Space-borne Bose-Einstein condensation for precision interferometry[J]. *Nature*, 2018, 562(7727): 391-395.
- [24] Corgier R, Amri S, Herr W, et al. Fast manipulation of Bose-Einstein condensates with an atom chip[J]. *New Journal of Physics*, 2018, 20(5): 055002.
- [25] Aveline D C, Williams J R, Elliott E R, et al. Observation of Bose-Einstein condensates in an Earth-orbiting research lab[J]. *Nature*, 2020, 582(7811): 193-197.
- [26] Deppe C, Herr W, Cornelius M, et al. Collective-mode enhanced matter-wave optics[J]. *Physical Review Letters*, 2021, 127(10): 100401.
- [27] Gaaloul N, Meister M, Corgier R, et al. A space-based quantum gas laboratory at picokelvin energy scales[EB/OL]. (2022-01-18)[2021-02-05]. <https://arxiv.org/abs/2201.06919>.
- [28] Wang L, Zhang P, Chen X Z, et al. Generating a picokelvin ultracold atomic ensemble in microgravity[J]. *Journal of Physics B: Atomic, Molecular and Optical Physics*, 2013, 46(19): 195302.
- [29] Yao H P, Luan T, Li C, et al. Comparison of different techniques in optical trap for generating picokelvin 3D atom cloud in microgravity[J]. *Optics Communications*, 2016, 359: 123-128.
- [30] Luan T, Li Y F, Zhang X S, et al. Realization of two-stage crossed beam cooling and the comparison with Delta-kick cooling in experiment[J]. *Review of Scientific Instruments*, 2018, 89(12): 123110.

- [31] 洪毅, 侯霞, 陈迪俊, 等. 基于 Rb^{87} 调制转移光谱稳频技术研究[J]. 中国激光, 2021, 48(21): 2101003.
Hong Y, Hou X, Chen D J, et al. Research on frequency stabilization technology of modulation transfer spectroscopy based on Rb^{87} [J]. Chinese Journal of Lasers, 2021, 48(21): 2101003.
- [32] Liu Q, Xie Y, Li L, et al. Development of an ultra-high vacuum system for a cold atom physics rack in space[J]. Vacuum, 2021, 190: 110192.
- [33] 刘乾, 谢昱, 李琳, 等. 基于人工神经网络的超冷原子实验多参数自主优化系统[J]. 中国激光, 2021, 48(24): 2412001.
Liu Q, Xie Y, Li L, et al. Multiparameter autonomous optimization system for ultracold atomic experiments based on artificial neural network[J]. Chinese Journal of Lasers, 2021, 48(24): 2412001.
- [34] 刘乾, 谢昱, 李琳, 等. 基于红失谐高斯光束的冷原子束流长距离传输[J]. 光学学报, 2021, 41(21): 2102001.
Liu Q, Xie Y, Li L, et al. Long-distance transmission of cold atomic beams based on red-detuned Gaussian beams[J]. Acta Optica Sinica, 2021, 41(21): 2102001.
- [35] Arnold K J, Barrett M D. All-optical Bose-Einstein condensation in a $1.06 \mu\text{m}$ dipole trap[J]. Optics Communications, 2011, 284(13): 3288-3291.
- [36] Condon G, Rabault M, Barrett B, et al. All-optical Bose-Einstein condensates in microgravity[J]. Physical Review Letters, 2019, 123(24): 240402.
- [37] Savard T A, O'Hara K M, Thomas J E. Laser noise induced heating in far off resonance optical traps[J]. Physical Review A, 1997, 56(2): R1095-R1098.

Development of Integrated All-Fiber 1064 nm Laser System for Ultracold Atomic Cooling

Xie Yu^{1,2}, Liang Ang^{1,2}, Li Wenwen^{1,2}, Huang Mingshan^{1,2}, Wang Bin^{1**}, Liu Liang^{1*}

¹Aerospace Laser Engineering Department, Shanghai Institute of Optics and Fine Mechanics, Chinese Academy of Sciences, Shanghai 201800, China;

²College of Materials Science and Opto-Electronic Technology, University of Chinese Academy of Sciences, Beijing 100049, China

Abstract

Objective Deep cooling is a key step in the preparation of ultracold atoms and a key technology for exploring extremely low temperatures. To rule out the effect of gravity, scientists combined microgravity experiments with atomic cooling experiments to get even colder temperatures below 1 nK. The Cold Atom Physics Research rack in the Chinese space station will adopt the deep cooling scheme of all-optical two-stage cooling (TSC) proposed by Chen Xuzong's research group at Peking University. In this scheme, two pairs of 1064 nm Far-Off Resonant optical-dipole Traps (FORTs) are used to successively cool ^{87}Rb atomic cloud by evaporative cooling and adiabatic expansion cooling. According to a direct Monte Carlo simulation, it is concluded that ultracold atomic gas below 100 pK can be obtained in microgravity environments by TSC process. In order to cover the experimental requirements in orbit, we develop a set of integrated optical-fiber 1064-nm laser system. This system provides four high power, high dynamic range, and low relative intensity noise (RIN) 1064-nm infrared channels, with full digitalization, high integration, high stability, and easy maintenance, which fully meets the application requirements of the space station and other remote-control projects.

Methods The system adopts beam splitting amplification scheme, namely, "pre-amplifiers+beam splitters +power controlling+post-amplifiers", to carry out multi-channel, high-power amplified, and high-dynamic range-controlled laser sources which is generated from a single seed light.

This laser system composed of polarization-maintaining fiber devices, as shown in Fig. 1, can be divided into two stages. The first stage, "high-quality seed source", as shown in left purple shadow of Fig. 1, consists of three parts: a seed source, a high-gaining pre-amplifier (PA), and cascade fiber beam splitters, and it is used to provide stable and narrow-linewidth seed light required by the subsequent optical operations. The other stage, "high-power amplification", as shown in right shadow of Fig. 1, consists of two components: a power control level, consisting of boost amplifiers (BO) and fiber-coupled acousto-optic modulator (AOM), and a power monitoring level, consisting of terminal photodiodes, and it plays the role of amplifying, output controlling, and power feedback, so that the output signals meet the experimental requirements in terms of high power, high dynamic range, high stability, and low RIN. From the left to right in Fig. 1, the continuous-wave seed signal, coming from a single-mode narrow 1064-nm laser tube, is sequentially amplified, filtered, split, and controlled within this full-functional optical platform to generate four 1064-nm FORTs, CH1-CH4, where CH1 and CH2 are called as high-power thin-waisted FORTs, and CH3 and CH4 are named after low-power wide-waisted FORTs.

As for the design of amplifiers, our laser adopts the full-fiber Master Oscillation Power Amplifier (MOPA) scheme to enlarge the optical power, where ytterbium-doped fibers (YDFs) with emission band from 1000 nm to 1100 nm are selected as the gain medium in the application of ^{87}Rb TSC and a 976-nm wavelength-locked laser diode is used for cladding forward pumping of these YDF. Both of PA and BOs are adopted a one-level MOPA scheme, as present in Fig. 2, to amplify and control the gained beams. With these amplifiers and power feedback mechanism, the laser system has capability of producing multi-channel laser with high power and low noisy, which satisfies the TSC experimental requirements.

Results and Discussions We run a series of tests to evaluate the performance of the laser system in terms of output power, spectrum, stability, RIN, etc. and conduct ground-based TSC pre-experiments to verify the overall system design in real experimental environments. The results show that this system has realized two 5-W and two 160-mW optical power independent output channels, has performed its capability of 60-dB high power-scanning dynamic range, as shown in Table 1, and has reduced the RIN as low as 5×10^{-4} , as demonstrated in Fig. 6. In the subsequent ground TSC experiments, we have obtained an ultra-cold ^{87}Rb atomic cluster with an extreme-low temperature of 10 nK, which is much lower than the cooling temperature in general all-optical evaporative cooling, and the experimental results are presented in Fig. 7 in details. All the tests and experiments indicate that our laser system reaches the overall performance requirements and is competent in future in-orbit TSC experiments.

Conclusions In this paper, we describe in detail the development and testing of an integrated all fiber 1064-nm laser system for ^{87}Rb atomic deep cooling. The system uses all optical fiber devices to realize the functions of seed source, optical power amplification, and optical power feedback controlling. It has the characteristics of digitalization and integration, and it is suitable for various applications of ultracold atoms with mobile requirements. The performance evaluation and experimental results prove that the laser system fully meets the power, control, and stability requirements of the TSC deep cooling experiments on four beams of optical dipole traps. This laser system has been installed in the Cold Atom Physics Research rack in Chinese Space Station, has been launched in October 2022, and plays an important role in ultracold physics researches in orbit.

Key words laser optics; laser trapping; Bose-Einstein condensate; optical fiber laser; laser cooling